

# $\eta$ mesons in hot and dense asymmetric nuclear matter

Rajesh Kumar<sup>\*</sup> and Arvind Kumar<sup>†</sup>

*Department of Physics, Dr. B R Ambedkar National Institute  
of Technology Jalandhar, Jalandhar – 144011, Punjab, India*

## Abstract

We study the  $\eta N$  interactions in the hot and dense isospin asymmetric nuclear matter using two different approaches. In the first approach, the in-medium mass and optical potential of  $\eta$ -meson have been calculated in the chiral SU(3) model, considering the effect of explicit symmetry breaking term and range terms in the  $\eta N$  interaction Lagrangian density. In the second scenario, the conjunction of chiral perturbation theory and chiral SU(3) model is employed. In this case, the next-to-leading order  $\eta N$  interactions are evaluated from the chiral perturbation theory (ChPT), and the in-medium contribution of scalar densities are taken as input from chiral SU(3) model. We observe a larger negative mass-shift in the ChPT+chiral model approach compared to the chiral SU(3) model alone as a function of nuclear density. Moreover, the increase in the asymmetry and temperature cause a decrease in the magnitude of mass-shift. We have also studied the impact of  $\eta N$  scattering length  $a^{\eta N}$  on the  $\eta$  meson mass  $m_\eta^*$  and observed that the  $m_\eta^*$  decrease more for increasing the value of scattering length.

---

<sup>\*</sup>Electronic address: [rajesh.sism@gmail.com](mailto:rajesh.sism@gmail.com)

<sup>†</sup>Electronic address: [kumara@nitj.ac.in](mailto:kumara@nitj.ac.in)

## I. INTRODUCTION

The meson-baryons interactions are very imperative topic of research to study the physics of non-perturbative QCD regime [1–12]. The heavy ion-collisions (HICs) are used to study the strong-interaction physics by colliding high energy particles. As a byproduct of the collision, the Quark Gluon Plasma (QGP) appears under the utmost conditions of density and temperature [12]. Afterward with the expansion of fireball the QGP cools down and changes its phase to the hadronic matter through hadronization process [12]. These two regimes *i.e.* QGP phase and hadronic phase have different characterization of the respective medium. For example, in the former phase quarks and gluons act as a degree of freedom whereas in the latter, mesons and baryons play this role. In QGP phase the chiral symmetry is followed ( $m_q \sim 0$ ) but in hadronic phase it is broken explicitly ( $m_q \neq 0$ ) and spontaneously ( $\langle \bar{q}q \rangle \neq 0$ ) [12, 13]. Furthermore, in the hadronic ensemble, the thermodynamics quantities namely nuclear density (number density of nucleons), isospin asymmetry (number of neutrons vs the number of protons), and temperature also play a crucial role to modify the in-medium properties of the mesons and baryons [1, 2, 12]. The operation of future experimental facilities such as CBM and PANDA at GSI, Germany, NICA at Dubna, Russia and, J-PARC at Japan may lead to considerable progress in the understanding of meson-baryons interactions [12, 13].

On the theoretical side, several potential models have been theorized to study the physics of the non-perturbative regime. Some of these are: Nambu-Jona-Lasinio (NJL) model [14], the Polyakov loop extended NJL (PNJL) model [15–17], chiral perturbation theory (ChPT) [5, 10], coupled channel approach [1, 6–8, 18], chiral  $SU(3)$  model [2, 19–21, 21–28], Quark-Meson Coupling (QMC) model [29–34], Polyakov Quark Meson (PQM) model [35, 36], and QCD sum rules [3, 37–41], etc. Various effective models are formulated keeping in view the fundamental QCD properties such as broken scale invariance and spontaneous and explicit breaking of the chiral symmetry.

For the first time, Haider and Liu anticipated that the  $\eta N$  interactions are attractive and suggested the possibility of  $\eta$ -meson bound states [42, 43]. The negative mass-shift/optical potential of  $\eta$ -meson has attracted researchers to study the possibilities of  $\eta$ -mesic nuclei formation [5, 10, 11]. At nuclear saturation density, the optical potential of -20 MeV was anticipated in the chiral coupled channel approach, considering leading order terms [11].

Using same coupled channel model, Chiang *et.al.* obtained optical potential  $U_\eta = -34$  MeV in the normal nuclear matter, assuming the  $\eta N$  interactions dominated by  $N^*(1535)$  excitation [44] and anticipated that the attractive potential can produce  $\eta$ -meson bound state with light and heavy nucleus. Using the QMC model, authors of Ref. [45] obtained optical potential -60 MeV at  $\rho_N = \rho_0$ . The chiral unitary approach was also implied to evaluate the  $\eta$  potential and it was observed to be -54 MeV [46]. A more deep optical potential of -72 MeV was observed in Ref. [47]. In this article the possibility of a bound state with  $\eta$ -meson was also explored.

In Ref. [10], using  $\eta N$  Lagrangian off-shell terms, at normal nuclear density, the in-medium mass of  $\eta$ -meson was found to be  $(0.84 \pm 0.015)m_\eta$  and the corresponding optical potential was observed as  $-(83 \pm 5)$  MeV. Furthermore, using the relativistic mean-field theory, Song *et al.* observed the optical potential by varying the scattering length [48]. Clearly, the values of  $\eta$  optical potential predicted in various studies varies over large range, *i.e.*, -20 MeV to -85 MeV and hence, have considerable model dependence. In addition to theoretical attempts, there are experimental studies to explore the properties of  $\eta$  mesons [49–54]. For example, for different  $\eta$  hadron interactions, the  $\eta$ -meson production has been studied in Refs. [49–51] and the transverse momentum spectra of  $\eta$ -meson is measured in HICs near the free  $N$ - $N$  production threshold [51].

In the current investigation, we present the in-medium mass and optical potential of the  $\eta$ -meson in hot and dense asymmetric nuclear matter using chiral SU(3) model. By incorporating the medium induced nucleon scalar densities, we calculate the in-medium mass-shift of  $\eta$ -meson using the  $\eta N$  effective Lagrangian of chiral SU(3) model. Furthermore, as discussed earlier, the in-medium mass and optical potential of  $\eta$ -meson have been studied using the unitary approach of ChPT and relativistic mean-field model [10, 48]. Following this work, as a second part of the current investigation the effective mass of  $\eta$ -meson is also evaluated using the chiral  $\eta N$  Lagrangian of chiral perturbation theory [10]. In this approach, the nucleon scalar densities are calculated from chiral SU(3) model and plugged in the dispersion relation of  $\eta N$  interactions derived from ChPT Lagrangian.

The chiral SU(3) model is extensively used to explore the in-medium properties of the mesons and baryons in the hot and dense hadronic matter [19, 21, 55]. For example, the model was used to study the in-medium mass and optical potential of kaons, antikaons and phi mesons in the nuclear and hyperonic matter [19, 22, 26]. Furthermore, in the nuclear

and hadronic matter the in-medium mass of spin 0, spin 1  $D$  mesons and quarkonia were calculated using the conjunction of chiral  $SU(3)$  model and QCD sum rules with [23–25, 56] and without taking the effect of magnetic field [21, 57–60]. The model was extended to  $SU(4)$  and  $SU(5)$  sector to evaluate the medium induced properties of heavy mesons such as  $D$  and  $B$  [22, 27, 28]. On the other hand, the chiral perturbation theory is also a successful theoretical framework to study the baryon-meson interactions. The in-medium properties of  $K$  meson were first studied by Kaplan and Nelson using chiral perturbation theory (ChPT) [4]. The same theory was applied to study the  $\eta$ -nucleon interactions via adding leading order terms in the model Lagrangian [5]. The heavy baryon chiral perturbation theory was also applied to study the kaon condensation which is an imperative property to study the neutron star matter [61–63]. The ChPT theory was also improved by the introduction of next-to-leading order terms in the chiral effective Lagrangian. By including these off-shell terms, Zhong *et.al.* anticipated appreciable decrease in the in-medium mass of  $\eta$ -meson which is favorable for the formation of  $\eta$ -mesic nuclei [10].

The layout of the present paper is as follows: In the next section, we will give brief explanation of the formalism used in the present work. In section II A 1, we will derive the  $\eta N$  interactions in the chiral  $SU(3)$  model whereas, in section II A 2,  $\eta N$  methodology will be given in the unified approach of chiral perturbation theory and chiral model. In section III, we will discuss the in-medium effects on the mass of  $\eta$ -meson, and finally in section IV, we will present the summary.

## II. FORMALISM

### A. IN-MEDIUM SCALAR FIELDS IN THE CHIRAL $SU(3)$ MODEL

The Lagrangian density of the chiral  $SU(3)$  model is written as

$$\mathcal{L}_{\text{chiral}} = \mathcal{L}_{\text{kin}} + \sum_{M=S,V} \mathcal{L}_{NM} + \mathcal{L}_{\text{vec}} + \mathcal{L}_0 + \mathcal{L}_{SB}. \quad (1)$$

The model preserves the fundamental QCD properties such as the broken scale invariance and non-linear realization of the chiral symmetry [2, 23, 24, 64–67]. It is successfully used to explain the nuclear matter, finite nuclei, neutron star, and hypernuclei [2, 23, 24, 64–67]. In this model, the nucleons and baryons interact by the exchange of the vector fields  $\omega$  and

$\rho$  along with the scalar fields  $\sigma$ ,  $\zeta$  and  $\delta$  in the nuclear medium. The vector fields give short-range repulsion or attraction which depends on the type of meson-nucleon interaction whereas the scalar fields give attractive contributions to the medium [26]. The  $\sigma$  field is a non-strange scalar-isoscalar field which represents the scalar mesons  $\sigma (u\bar{d})$  whereas the  $\zeta$  field is a strange scalar-isoscalar field which represent the scalar meson  $(s\bar{s})$  [68]. Moreover, the scalar-isovector field  $\delta \sim (\bar{u}u - \bar{d}d)$  is incorporated in the present model to study the effect of the isospin asymmetric matter. Further, the glueball field,  $\chi$  is a hypothetical gluon field that contains gluon particles and is introduced in the chiral models to incorporate the scale invariance property of QCD [2, 69]. We have used mean-field approximation to simplify the model by neglecting the effect of quantum and thermal fluctuations near phase transitions [23, 70].

In Eq.(1), the  $\mathcal{L}_{kin}$  term describes the the kinetic energy term and the second term  $\mathcal{L}_{NM}$  given by

$$\mathcal{L}_{NM} = - \sum_i \bar{\psi}_i [m_i^* + g_{\omega i} \gamma_0 \omega + g_{\rho i} \gamma_0 \rho] \psi_i, \quad (2)$$

defines the nucleon-meson interactions with in-medium nucleon mass as

$$m_i^* = -(g_{\sigma i} \sigma + g_{\zeta i} \zeta + g_{\delta i} \tau_3 \delta), \quad (3)$$

where  $\tau_3$  denotes the 3<sup>rd</sup> component of isospin and  $g_{\sigma i}$ ,  $g_{\zeta i}$  and  $g_{\delta i}$  are the coupling constants of  $\sigma$ ,  $\zeta$  and field  $\delta$  with nucleons ( $i=p, n$ ), respectively. The next term  $\mathcal{L}_{vec}$  is given by

$$\mathcal{L}_{vec} = \frac{1}{2} (m_\omega^2 \omega^2 + m_\rho^2 \rho^2) \frac{\chi^2}{\chi_0^2} + g_4 (\omega^4 + 6\omega^2 \rho^2 + \rho^4), \quad (4)$$

reproduces the mass of vector mesons through self-interactions. The  $\mathcal{L}_0$  defines the spontaneous chiral symmetry breaking by the equation

$$\begin{aligned} \mathcal{L}_0 = & -\frac{1}{2} k_0 \chi^2 (\sigma^2 + \zeta^2 + \delta^2) + k_1 (\sigma^2 + \zeta^2 + \delta^2)^2 \\ & + k_2 \left( \frac{\sigma^4}{2} + \frac{\delta^4}{2} + 3\sigma^2 \delta^2 + \zeta^4 \right) + k_3 \chi (\sigma^2 - \delta^2) \zeta \\ & - k_4 \chi^4 - \frac{1}{4} \chi^4 \ln \frac{\chi^4}{\chi_0^4} + \frac{d}{3} \chi^4 \ln \left( \left( \frac{(\sigma^2 - \delta^2) \zeta}{\sigma_0^2 \zeta_0} \right) \left( \frac{\chi}{\chi_0} \right)^3 \right). \end{aligned} \quad (5)$$

In this equation, the  $\sigma_0$ ,  $\zeta_0$ ,  $\delta_0$  and  $\chi_0$  denote the vacuum values of  $\sigma$ ,  $\zeta$ ,  $\delta$  and  $\chi$  scalar fields, respectively. Also, the parameter  $d=0.064$  along with  $k_i$  ( $i = 1$  to  $4$ ) and other medium parameters are fitted to regenerate the vacuum values of scalar and vector fields,  $\eta$ ,  $\eta'$  mesons and the nucleon mass [2, 21, 24]. In table I, we have tabulated the values of various parameters. Furthermore, the last term  $\mathcal{L}_{SB}$  in Eq.(1) describes the explicit chiral symmetry breaking property and is written as

$$\mathcal{L}_{SB} = - \left( \frac{\chi}{\chi_0} \right)^2 \left[ m_\pi^2 f_\pi \sigma + (\sqrt{2} m_K^2 f_K - \frac{1}{\sqrt{2}} m_\pi^2 f_\pi) \zeta \right]. \quad (6)$$

In the above equation,  $m_\pi$ ,  $m_K$ ,  $f_\pi$ , and  $f_K$  symbolize the masses and decay constants of pions and kaons, respectively.

The non-linear coupled equations of motion of the scalar and vector fields are deduced by solving the total Lagrangian (Eq.(1)) using the Euler-Lagrange equations [24, 25] and are given as

$$k_0 \chi^2 \sigma - 4k_1 (\sigma^2 + \zeta^2 + \delta^2) \sigma - 2k_2 (\sigma^3 + 3\sigma\delta^2) - 2k_3 \chi \sigma \zeta - \frac{d}{3} \chi^4 \left( \frac{2\sigma}{\sigma^2 - \delta^2} \right) + \left( \frac{\chi}{\chi_0} \right)^2 m_\pi^2 f_\pi = \sum g_{\sigma i} \rho_i^s, \quad (7)$$

$$k_0 \chi^2 \zeta - 4k_1 (\sigma^2 + \zeta^2 + \delta^2) \zeta - 4k_2 \zeta^3 - k_3 \chi (\sigma^2 - \delta^2) - \frac{d}{3} \frac{\chi^4}{\zeta} + \left( \frac{\chi}{\chi_0} \right)^2 \left[ \sqrt{2} m_K^2 f_K - \frac{1}{\sqrt{2}} m_\pi^2 f_\pi \right] = \sum g_{\zeta i} \rho_i^s, \quad (8)$$

$$k_0 \chi^2 \delta - 4k_1 (\sigma^2 + \zeta^2 + \delta^2) \delta - 2k_2 (\delta^3 + 3\sigma^2 \delta) + 2k_3 \chi \delta \zeta + \frac{2}{3} d \chi^4 \left( \frac{\delta}{\sigma^2 - \delta^2} \right) = \sum g_{\delta i} \tau_3 \rho_i^s, \quad (9)$$

$$\left( \frac{\chi}{\chi_0} \right)^2 m_\omega^2 \omega + g_4 (4\omega^3 + 12\rho^2 \omega) = \sum g_{\omega i} \rho_i^v, \quad (10)$$

$$\left( \frac{\chi}{\chi_0} \right)^2 m_\rho^2 \rho + g_4 (4\rho^3 + 12\omega^2 \rho) = \sum g_{\rho i} \tau_3 \rho_i^v, \quad (11)$$

and

$$\begin{aligned}
& k_0 \chi (\sigma^2 + \zeta^2 + \delta^2) - k_3 (\sigma^2 - \delta^2) \zeta + \chi^3 \left[ 1 + \ln \left( \frac{\chi^4}{\chi_0^4} \right) \right] + (4k_4 - d) \chi^3 \\
& - \frac{4}{3} d \chi^3 \ln \left( \left( \frac{(\sigma^2 - \delta^2) \zeta}{\sigma_0^2 \zeta_0} \right) \left( \frac{\chi}{\chi_0} \right)^3 \right) + \frac{2\chi}{\chi_0^2} \left[ m_\pi^2 f_\pi \sigma + \left( \sqrt{2} m_K^2 f_K - \frac{1}{\sqrt{2}} m_\pi^2 f_\pi \right) \zeta \right] \\
& - \frac{\chi}{\chi_0^2} (m_\omega^2 \omega^2 + m_\rho^2 \rho^2) = 0, \quad (12)
\end{aligned}$$

respectively.

In above equations, the  $\rho_i^s$  and  $\rho_i^v$  denote the scalar and vector densities of  $i^{th}$  nucleons ( $i = n, p$ ) [2, 24] and are given as

$$\rho_i^v = \gamma_i \int \frac{d^3 k}{(2\pi)^3} \left( \frac{1}{1 + \exp [\beta(E_i^*(k) - \mu_i^*)]} - \frac{1}{1 + \exp [\beta(E_i^*(k) + \mu_i^*)]} \right), \quad (13)$$

and

$$\rho_i^s = \gamma_i \int \frac{d^3 k}{(2\pi)^3} \frac{m_i^*}{E_i^*(k)} \left( \frac{1}{1 + \exp [\beta(E_i^*(k) - \mu_i^*)]} + \frac{1}{1 + \exp [\beta(E_i^*(k) + \mu_i^*)]} \right), \quad (14)$$

respectively, where  $\beta = \frac{1}{kT}$ ,  $E_i^*(k) = \sqrt{k^2 + m_i^{*2}}$ ,  $\mu_i^* = \mu_i - g_{\omega i} \omega - g_{\rho i} \tau_3 \rho$  and  $\gamma_i$  is the degeneracy factor. Moreover, the isospin effect on the scalar and vector density is measured by the definition,  $I = -\frac{\sum_i \tau_{3i} \rho_i^v}{2\rho_N}$ . In the next section, we calculate the medium-modified mass of  $\eta$  mesons in hot asymmetric nuclear matter. The medium modified  $\eta$  meson mass is evaluated from the dispersion relation which is obtained from the  $\eta N$  equation of motion.

### 1. $\eta N$ INTERACTIONS IN THE CHIRAL $SU(3)$ MODEL

In the chiral  $SU(3)$  model, the  $\eta N$  interaction Lagrangian density can be written as

$$\begin{aligned}
\mathcal{L}_\eta &= \left( \frac{1}{2} - \frac{\sigma' + 4\zeta'(2f_K - f_\pi)}{\sqrt{2}f^2} \right) \partial^\mu \eta \partial_\mu \eta \\
&- \frac{1}{2} \left( m_\eta^2 - \frac{(\sqrt{2}\sigma' - 4\zeta')m_\pi^2 f_\pi + 8\zeta' m_K^2 f_K}{\sqrt{2}f^2} \right) \eta^2 \\
&+ \frac{d'}{f^2} \left( \frac{\rho_p^s + \rho_n^s}{4} \right) \partial^\mu \eta \partial_\mu \eta, \quad (15)
\end{aligned}$$

The above chiral  $\eta N$  Lagrangian consists of three terms.

$k_0$	$k_1$	$k_2$	$k_3$	$k_4$
2.53	1.35	-4.77	-2.77	-0.218
$\sigma_0$ (MeV)	$\zeta_0$ (MeV)	$\chi_0$ (MeV)	$d$	$\rho_0$ (fm <sup>-3</sup> )
-93.29	-106.8	409.8	0.064	0.15
$g_{\sigma N}$	$g_{\zeta N}$	$g_{\delta N}$	$g_{\omega N}$	$g_{\rho N}$
10.56	-0.46	2.48	13.35	5.48
$m_\pi$ (MeV)	$m_K$ (MeV)	$f_\pi$ (MeV)	$f_K$ (MeV)	$g_4$
139	498	93.29	122.14	79.91
$m_\sigma$ (MeV)	$m_\zeta$ (MeV)	$m_\delta$ (MeV)	$M_N$ (MeV)	$m_\eta$ (MeV)
466.5	1024.5	899.5	939	574.374

Table I: Different constants used in the present work [2].

- First Range Term:

The first term in the chiral Lagrangian describes the first range term [2, 22] and is obtained from

$$\mathcal{L}_{1\text{strangeterm}} = Tr(u_\mu X u^\mu X + X u_\mu u^\mu X). \quad (16)$$

In the above equation,  $u_\mu = -\frac{i}{2} [u^\dagger(\partial_\mu u) - u(\partial_\mu u^\dagger)]$  and  $u = \exp\left[\frac{i}{\sqrt{2}\sigma_0} P \gamma_5\right]$ , which is expanded up to second order. Here, symbols  $X$  and  $P$  represent the scalar and pseudoscalar meson matrices [2], respectively and are explicitly given by Eqs. (A1) and (A2) in the appendix A. Furthermore, the vacuum values of  $\sigma$  and  $\zeta$  fields are deduced in terms of pions and kaons decay constant by solving the axial current of pions and kaons [2] through relation

$$\sigma_0 = -f_\pi \quad \zeta_0 = -\frac{1}{\sqrt{2}}(2f_K - f_\pi). \quad (17)$$

Moreover, in the first term of  $\eta N$  Lagrangian  $\sigma' (= \sigma - \sigma_0)$ ,  $\zeta' (= \zeta - \zeta_0)$  and  $\delta' (= \delta - \delta_0)$  define the digression of the expectation values of fields from their vacuum expectations. Also,  $f = \sqrt{f_\pi^2 + 2(2f_K - f_\pi)^2}$  and  $d' = 3d_1 + d_2$  are the constant parameters.

- Mass Term:

Further, the mass term of the chiral model gives the second term of  $\eta N$  Lagrangian and is given by



$$\mathcal{L}_{SB} = -\frac{1}{2}\text{Tr}A_p (\bar{u}Xu + u^\dagger Xu^\dagger), \quad (18)$$

where  $A_p$  is a diagonal matrix given in the Eq.(A3). The vacuum mass of  $\eta$  meson,  $m_\eta$ , is extracted from the above term and is given by the relation

$$m_\eta = \frac{1}{f} \sqrt{\left(3m_\pi^2 f_K m_K^2 + \frac{8f_K^2 m_K^2}{f_\pi^2} - \frac{4f_K m_\pi^2}{f_\pi}\right)}. \quad (19)$$

Substituting the values of various constants in above  $m_\eta$  turns out to be 574.374 MeV which is with an accuracy of 4.9 % of physical mass *i.e.* 547.862 MeV [71]. The vacuum mass of  $\eta$ -meson has model dependency [72] but here in the present work, we are more concerned in the  $\eta$  in-medium mass-shift which is nearly same for both the masses. In Ref. [72], using Gell-Mann Okubo mass formula under octet approximation in the SU(4) meson multiplets, authors calculated the vacuum mass of  $\eta$ -meson to be 567 MeV which is with an accuracy of 3.6 %.

- $d'$  Term:

The third term (*i.e.*  $d'$  term) in the  $\eta N$  Lagrangian originates from the baryon-meson interaction Lagrangian densities [20, 27]

$$\mathcal{L}_{d_1}^{BM} = \frac{d_1}{2} \text{Tr}(u_\mu u^\mu) \text{Tr}(\bar{B}B), \quad (20)$$

and

$$\mathcal{L}_{d_2}^{BM} = d_2 \text{Tr}(\bar{B}u_\mu u^\mu B). \quad (21)$$

In above,  $B$  denotes the baryon matrix (see Eq.(A4)).

It should be noted that in case of  $\eta N$  interactions of Eq. (15), the terms corresponding to vectorial Weinberg-Tomozawa term vanishes. On the the other hand, the Weinberg-Tomozawa term plays a crucial role in the determination of  $K(\bar{K})$  and  $D(\bar{D})$  in-medium mass [22, 28].

Using the  $\eta N$  Lagrangian in the Euler-Lagrange equation for  $\eta$  meson, the equation of motion is evaluated as

$$\begin{aligned} & \partial^\mu \partial_\mu \eta - \left( m_\eta^2 - \frac{(\sqrt{2}\sigma' - 4\zeta')m_\pi^2 f_\pi + 8\zeta' m_K^2 f_K}{\sqrt{2}f^2} \right) \eta \\ & + \frac{2d'}{f^2} \left( \frac{\rho_p^s + \rho_n^s}{4} - \frac{\sigma' + 4\zeta'(2f_K - f_\pi)}{\sqrt{2}} \right) \partial^\mu \partial_\mu \eta = 0. \end{aligned} \quad (22)$$

Performing the Fourier transformation on the above equation, the dispersion relation for  $\eta$  meson turns out to be

$$-\omega^2 + \mathbf{k}^2 + m_\eta^2 - \Pi^*(\omega, |\mathbf{k}|) = 0. \quad (23)$$

In the above equation,  $\Pi^*$  denotes the effective self-energy of  $\eta$  meson, explicitly given as

$$\begin{aligned} \Pi^*(\omega, |\mathbf{k}|) = & -\frac{(\sqrt{2}\sigma' - 4\zeta')m_\pi^2 f_\pi + 8\zeta' m_K^2 f_K}{\sqrt{2}f^2} + \frac{2d'}{f^2} \left( \frac{\rho_p^s + \rho_n^s}{4} \right) (\omega^2 - \vec{k}^2) \\ & - \frac{2}{f^2} \left( \frac{\sigma' + 4\zeta'(2f_K - f_\pi)}{\sqrt{2}} \right) (\omega^2 - \mathbf{k}^2). \end{aligned} \quad (24)$$

The unknown parameter,  $d'$  is approximated from the experimental values of scattering length,  $a^{\eta N}$  [10]. In the chiral model, the expression of scattering length derived from the scattering amplitude is given by

$$\begin{aligned} a^{\eta N} = & \frac{1}{4\pi \left(1 + \frac{m_\eta}{M_N}\right)} \left[ \left( \frac{d'}{\sqrt{2}} - \frac{g_{\sigma N}}{m_\sigma^2} + \frac{4(2f_K - f_\pi)g_{\zeta N}}{m_\zeta^2} \right) \frac{m_\eta^2}{\sqrt{2}f^2} \right. \\ & \left. + \left( \frac{\sqrt{2}g_{\sigma N}}{m_\sigma^2} - \frac{4g_{\zeta N}}{m_\zeta^2} \right) \frac{m_\pi^2 f_\pi}{2\sqrt{2}f^2} + \tau_3 \frac{2\sqrt{2}g_{\delta N} m_K^2 f_K}{m_\delta^2 f^2} \right]. \end{aligned} \quad (25)$$

Rearranging the above for  $d'$  gives

$$\begin{aligned} d' = & \frac{f^2}{2\pi \left(1 + \frac{m_\eta}{M_N}\right)} \frac{a^{\eta N}}{m_\eta^2} + \frac{\sqrt{2}g_{\sigma N}}{m_\sigma^2} - \frac{4\sqrt{2}(2f_K - f_\pi)g_{\zeta N}}{m_\zeta^2} \\ & - \left( \frac{\sqrt{2}g_{\sigma N}}{m_\sigma^2} - \frac{4g_{\zeta N}}{m_\zeta^2} \right) \frac{m_\pi^2 f_\pi}{\sqrt{2}m_\eta^2} - \tau_3 \frac{4\sqrt{2}g_{\delta N} m_K^2 f_K}{m_\delta^2 m_\eta^2}. \end{aligned} \quad (26)$$

Using the condition,  $m_\eta^* = \omega(|\mathbf{k}|=0)$  in Eq. (23), we obtain the effective mass of  $\eta$  meson in the nuclear medium. Further, the momentum dependent optical potentials are defined through the relation [28, 73]

$$U_\eta^*(\omega, \mathbf{k}) = \omega(\mathbf{k}) - \sqrt{\mathbf{k}^2 + m_\eta^2}. \quad (27)$$

At zero momentum, the above equation gives

$$U_\eta^* = \Delta m_\eta^* = m_\eta^* - m_\eta. \quad (28)$$

2. UNIFICATION OF CHIRAL PERTURBATION THEORY (ChPT) AND CHIRAL MODEL

In this section, we discuss the unified approach of ChPT and chiral model to compute the in-medium mass of  $\eta$  mesons. The ChPT comprises the underlying chiral symmetry property of QCD and use an effective field theory approach [10]. The same theory along with Relativistic mean-field model has been used to deduce the eta-nucleon interactions in the symmetric nuclear matter [10, 48]. The Lagrangian density defining the meson-baryons interactions in this theory is given by

$$\mathcal{L}_{\text{ChPT}} = \mathcal{L}_P + \mathcal{L}_{PB}, \quad (29)$$

with  $P$  representing the pseudoscalar meson multiplet (see Eq.(A2)). Up to second chiral order, the  $\mathcal{L}_P$  term is defined as [4, 10]

$$\mathcal{L}_P = \frac{1}{4}f_\pi^2 \text{Tr} \partial^\mu \Sigma \partial_\mu \Sigma^\dagger + \frac{1}{2}f_\pi^2 B_0 \{ \text{Tr} M_q (\Sigma - 1) + \text{h.c.} \}, \quad (30)$$

where  $\Sigma = \xi^2 = \exp(i\sqrt{2}P/f_\pi)$  and  $M_q = \text{diag}\{m_q, m_q, m_s\}$  is the current quark mass matrix. The Lagrangian term,  $\mathcal{L}_{PB} = \mathcal{L}_{PB}^L + \mathcal{L}_{PB}^{NL}$  describes the leading and next to leading order contributions [4]. Jenkins and Manohar developed the next to leading order terms using heavy baryon chiral theory [5]. In this Lagrangian, the loop contributions are not considered as the higher-order corrections get suppressed for the small momentum scale,  $Q^2$  [10]. The different nuclear properties are studied successfully using  $\mathcal{L}_{PB}^{NL}$  [74].

The  $\eta N$  Lagrangian is obtained by expanding the Eq.(29) up to the second order of multiplet  $P$  [10]

$$\mathcal{L}_{\eta N} = \frac{1}{2} \partial^\mu \eta \partial_\mu \eta - \frac{1}{2} \left( m'_\eta{}^2 - \frac{\Sigma_{\eta N}}{f_\pi^2} \bar{\Psi}_N \Psi_N \right) \eta^2 + \frac{1}{2} \frac{\kappa}{f_\pi^2} \bar{\Psi}_N \Psi_N \partial^\mu \eta \partial_\mu \eta. \quad (31)$$

Here,  $m'_\eta = \sqrt{\frac{2}{3}B_0(m_q + 2m_s)}$  denotes the vacuum mass of  $\eta$  meson calculated in chiral perturbation theory. In the mass expression,  $B_0$  symbolize the relation with the order parameter of spontaneously broken chiral symmetry and  $m_{q(s)}$  denote the mass of light (strange) quarks [72]. For consistency with the chiral SU(3) model, we have used the same value of  $\eta$  meson vacuum mass *i.e.*  $m'_\eta = m_\eta = 574.374$  MeV in the further calculations of

ChPT. The  $\eta N$  sigma term  $\Sigma_{\eta N}$ , obtained from “ $a_i$ ” terms of the next-to-leading order chiral Lagrangian density is given as [10]

$$\Sigma_{\eta N} = -\frac{2}{3}[a_1 m_q + 4a_2 m_s + 2a_3(m_q + 2m_s)]. \quad (32)$$

The  $\Sigma_{\eta N}$  value is estimated to be  $280 \pm 130$  MeV from the different empirical observations of  $\Sigma_{KN}$  term having value  $380 \text{ MeV} \pm 100 \text{ MeV}$  [10, 61, 62, 75–79].

Also, the parameter  $\kappa$  in the last term of the Eq.(31) comprises the contributions from the “off-shell”  $d_i$  terms of the next to Leading order Lagrangian [10]. In the present work, we determined  $\kappa$  using the expression of  $\eta N$  scattering length,  $a^{\eta N}$ , calculated from the ChPT matrix amplitude (on-shell constraints) [10]

$$a^{\eta N} = \frac{1}{4\pi f_\pi^2(1 + m_\eta/M_N)} (\Sigma_{\eta N} + \kappa m_\eta^2), \quad (33)$$

and by re-arranging for  $\kappa$  it becomes

$$\kappa = 4\pi f_\pi^2 \left( \frac{1}{m_\eta^2} + \frac{1}{m_\eta M_N} \right) a^{\eta N} - \frac{\Sigma_{\eta N}}{m_\eta^2}. \quad (34)$$

We have taken the experimentally determined  $a^{\eta N}$  values *i.e.*  $0.91 \sim 1.14$  fm in the present investigation [10, 80–83]. Furthermore, the  $\eta N$  equation of motion has been derived using the interaction Lagrangian (Eq.(31)) in the Euler Lagrange equation of motion:

$$\left( \partial_\mu \partial^\mu + m_\eta^2 - \frac{\Sigma_{\eta N}}{2f_\pi^2} \langle \bar{\Psi}_N \Psi_N \rangle + \frac{\kappa}{2f_\pi^2} \langle \bar{\Psi}_N \Psi_N \rangle \partial_\mu \partial^\mu \right) \eta = 0. \quad (35)$$

In above,  $\langle \bar{\Psi}_N \Psi_N \rangle \equiv \rho_N^s = (\rho_p^s + \rho_n^s)$  defines the in-medium scalar density of nucleons calculated within the mean-field chiral SU(3) model (see Eqs.(13) and (14)). The Fourier transformation of Eq.(35) gives

$$-\omega^2 + \mathbf{k}^2 + m_\eta^2 - \frac{\Sigma_{\eta N}}{2f_\pi^2} \rho_N^s + \frac{\kappa}{2f_\pi^2} \rho_N^s (-\omega^2 + \mathbf{k}^2) = 0, \quad (36)$$

From the above equation, the effective mass  $m_\eta^* = \omega(|\mathbf{k}|=0)$  of  $\eta$  meson can be written as

$$m_\eta^* = \sqrt{\left( m_\eta^2 - \frac{\Sigma_{\eta N}}{2f_\pi^2} \rho_N^s \right) / \left( 1 + \frac{\kappa}{2f_\pi^2} \rho_N^s \right)}. \quad (37)$$

Further, the  $\eta$ -meson self-energy derived from Eq.(36) is given by

$$\Pi^*(\omega, \mathbf{k}) = \left( -\frac{\Sigma_{\eta N}}{2f_\pi^2} + \frac{\kappa}{2f_\pi^2} (-\omega^2 + \mathbf{k}^2) \right) \rho_N^s. \quad (38)$$

### III. RESULTS AND DISCUSSIONS

In this section, at first we discuss the behavior of in-medium nucleon scalar densities in the hot asymmetric nuclear matter. Further, we discuss the effective mass of  $\eta$  meson which is derived using the chiral SU(3) model alone in section III A and with the unified approach of ChPT and chiral SU(3) model in section III B . In both approaches, we show the results for range of scattering length,  $a^{nN}=0.91-1.14$  fm. Various parameters used in the present investigation are mentioned in table I.

In chiral model, the scalar densities of nucleons have been calculated through Eq. (14). This equation contains the effect of medium modified scalar and vector fields [2]. The in-medium behavior of these fields is obtained by solving the coupled equations of motion (Eqs. (7) to (12)) [26]. In fig. 1, we plot the scalar density of proton and neutron as a function of number density for finite values of temperature,  $T$  and isospin asymmetry parameter. In symmetric nuclear matter as the contribution of  $\delta$  and  $\rho$  field is zero [24], we get the same behavior of neutron and proton scalar densities. The  $\delta$  and  $\rho$  field changes the in-medium value of baryon mass  $m_i^*$  and effective chemical potential  $\mu_i^*$ , respectively which further modifies the nucleon scalar density (see Eq.(14)) [2]. In figure, at  $T = 0$  the scalar density increases linearly in the low density regime and becomes non-linear in the high density regime. When we move from  $I=0$  to  $I\neq 0$  region, we observe a gradual increase in the neutron scalar density whereas the proton scalar density decreases. This is because of the non-zero contribution of  $\delta$  and  $\rho$  field in the isospin asymmetric nuclear matter which changes the effective mass as well as chemical potential and therefore scalar density [2].

Another thermodynamic quantity *i.e.* temperature is also a main property of the nuclear medium and in fig. 1 we have shown how the in-medium dynamics changes under non-zero temperature. The effect of temperature is observed more in the high density regime as compared to the low density regime. For symmetric matter in sub-plots (a) and (c), we anticipate appreciable effect of temperature. Here, for a particular value of nuclear density the value of scalar densities decrease as a function of temperature. This is because of the Fermi distribution integral, due to the coupled nature of the equations (Eqs. (7) to (12)) the value of scalar density in Eq.(14) decreases when we increase the temperature in integral. On the other hand, in the highly asymmetric matter *i.e.*  $I=0.5$ , for the neutron scalar density the temperature effects become more appreciable. In addition, we observe a minor

contribution to the proton scalar density for higher temperature values. This is because at finite temperature the proton condensate ( $\bar{p}p$ ) *i.e.* proton scalar density still populates in the medium despite the zero value of proton number density  $\rho_p$ . The observed behavior of scalar densities in the symmetric nuclear matter is in agreement with the calculations of the Relativistic mean-field model [10, 48].

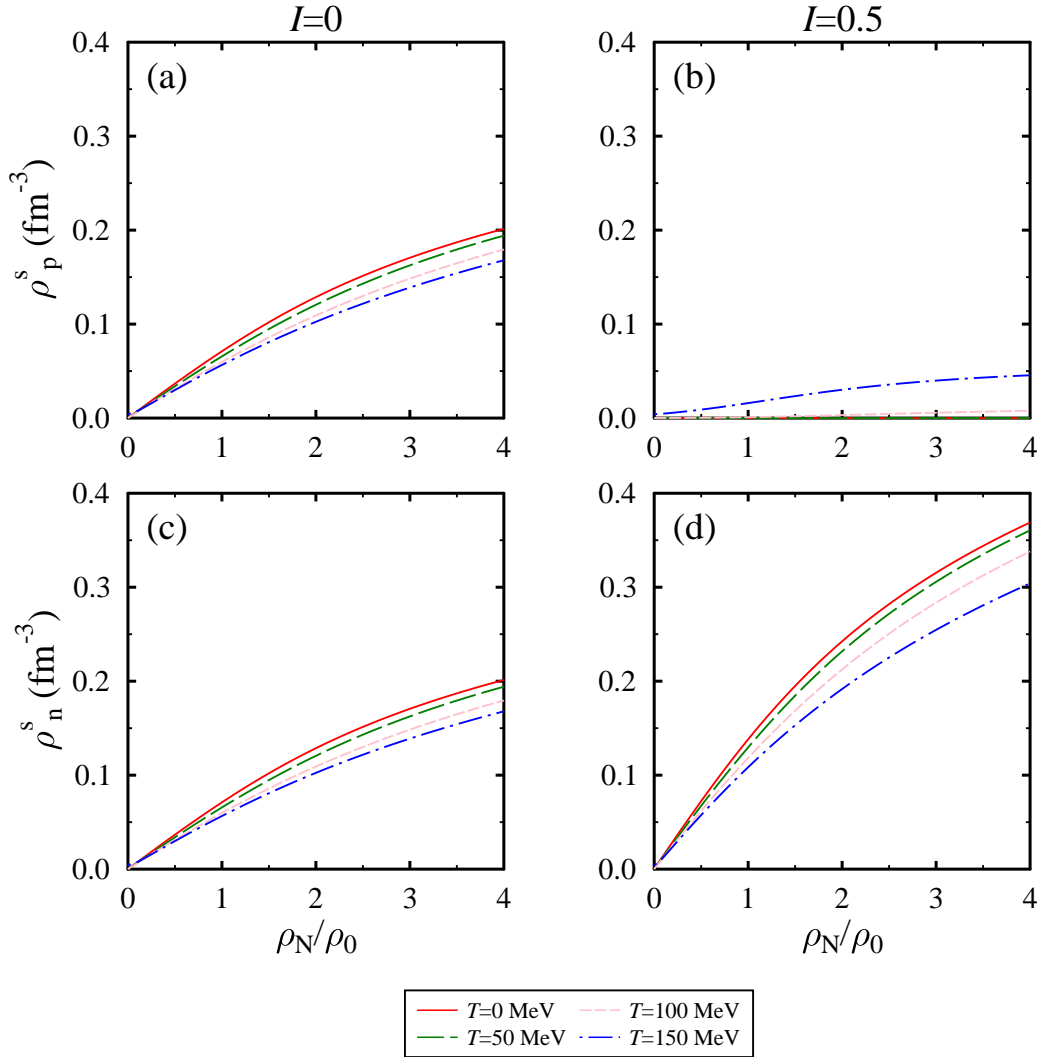


Figure 1: (Color online) The in-medium scalar density of nucleons.

	$a^{\eta N}$ (fm)	$\eta=0$				$\eta=0.5$			
		T=0		T=100		T=0		T=100	
		$\rho_0$	$4\rho_0$	$\rho_0$	$4\rho_0$	$\rho_0$	$4\rho_0$	$\rho_0$	$4\rho_0$
$\Delta m_\eta^*$	0.91	-46.18	-132.88	-37.78	-120.31	-44.74	-123.35	-37.74	-116.46
	1.02	-54.61	-146.77	-45.22	-133.79	-52.99	-136.93	-45.16	-129.78
	1.14	-63.37	-160.51	-52.98	-147.21	-61.58	-150.42	-52.92	-143.07

Table II: Values of in-medium mass-shift of  $\eta$ -meson for different medium attributes calculated in chiral model are tabulated (in units of MeV).

### A. Optical Potential and Mass of $\eta$ Meson in Chiral Model

In fig. 2, we have illustrated the medium modified mass of  $\eta$ -meson as a function of nuclear density for different values of scattering length. In the same figure, we also show the impact of isospin asymmetry and temperature. For given value of asymmetry, temperature, scattering length, the in-medium mass of  $\eta$ -meson is observed to decrease as a function of nuclear density. The rate of decrease is linear in the low density regime whereas in the high density regime it becomes non-linear. This behavior reflects the opposite variation of nucleon scalar density plotted in fig. 1. This is because the self-energy of  $\eta$ -meson (see Eq.(24)) has a direct dependence on the sum of scalar densities of nucleons. When we change the value of  $a^{\eta N}$  from 0.91 to 1.14 fm, we observe a decrement in the effective mass. For example, at  $\rho_N = \rho_0(4\rho_0)$ ,  $I=T=0$ , the effective mass of  $\eta$ -meson changes from 528 (441) to 512 (423) MeV when we change  $a^{\eta N}$  value from 0.91 to 1.14 fm, respectively. This is due to the  $d'$  term in Eq.(24). The  $d'$  term has direct dependence on  $a^{\eta N}$  as shown in Eq.(26) and therefore increasing the value of scattering length cause an increase in the value of  $d'$ . Due to the attractive contribution of the self-energy part corresponding to  $d'$  term the value of effective mass decreases. We also observed the substantial impact of the temperature on the in-medium mass in the symmetric nuclear matter which reflects the in-medium behavior of scalar densities. However, in the asymmetric nuclear matter, we observe the temperature effects on the mass to be less appreciable which reflects the less contribution of the net scalar density ( $\rho_p^s + \rho_n^s$ ).

The self-energy expression given by Eq.(24) contain three terms (i) first range term (ii) mass term and (iii)  $d'$  term. To understand the contribution of these individual terms, we

illustrated the in-medium mass of  $\eta$ -meson at zero and non-zero value of asymmetry and temperature in fig. 3 for these different terms. At zero temperature and asymmetry, one can see that the first range term gives an appreciable repulsive contribution to the effective mass whereas the mass and  $d'$  terms give attractive contributions. We observe the dominant contribution of  $d'$  term which in turn gets reflected in the net effective mass. For non-zero temperature and asymmetry, the variation in the  $d'$  term becomes less hence we get a lower value of effective mass. This is due to the effect of scalar density terms present in the  $d'$  term (Eq.(24)). For further understanding, in fig. 2 we plot the  $\eta$ -meson effective mass as a function of scattering length  $a^{\eta N}$  at  $\rho_N=\rho_0, 4\rho_0$ . At nuclear saturation density, we observe a linear decrease of effective mass with the increase in scattering length. Furthermore, the effective mass decrease more rapidly in the high density regime. The observed behaviour emphasizes the importance of scattering length in the  $\eta N$  interactions.

The decrease in the in-medium mass leads to a negative mass-shift which suggests the bound state formation of  $\eta$ -meson with a nucleus [5, 10]. To understand the bound state phenomenon, the study of in-medium optical potential is very imperative. By using the effective mass in Eq.(28), we plotted the optical potential of  $\eta$ -meson as a function of momentum  $|\mathbf{k}|$  for different values of  $\eta N$  scattering length and other medium parameters in figs. 5 to 7. In fig. 5, at  $\rho_N=\rho_0$  we observe a negative value of the optical potential. The value of optical potential becomes less negative as we increase the momentum of the  $\eta$ -meson. The variation of optical potential reflects the interplay between the effective mass and momentum. At high values of the momentum, Eq.(28) gets dominated by momentum and the contribution of effective mass becomes less.

A similar phenomenon happens in the high density regime. In this region, we observe appreciable values of optical potential which become less as momentum increases. Moreover, in the presence of a high density of neutron matter, we anticipate less effect of temperature which reflects the in-medium behavior of  $\eta$ -meson mass. In figs. 6 and 7 we observe a similar trend of optical potential with  $\eta$  momentum. In these figures, we observe a more negative value of optical potential as we increase the scattering length. As discussed earlier, the optical potential is directly related to in-medium mass, here it is illustrated to get a clear idea of negative potential. In the cold symmetric nuclear matter, at  $\rho_N=\rho_0(4\rho_0)$  we observe optical potential to be -54.61 (-146.77) MeV for  $a^{\eta N}=1.02$  fm, whereas for  $I=0.5$  these values changes to -52.99 (-136.93) MeV. For better understanding, we have tabulated



	$a^{\eta N}$ (fm)	$\eta=0$				$\eta=0.5$			
		T=0		T=100		T=0		T=100	
		$\rho_0$	$4\rho_0$	$\rho_0$	$4\rho_0$	$\rho_0$	$4\rho_0$	$\rho_0$	$4\rho_0$
$\Delta m_{\eta}^*$	0.91	-107.54	-219.71	-93.73	-205.06	-105.19	-208.52	-93.64	-200.43
	1.02	-116.83	-232.28	-102.21	-217.49	-114.35	-220.99	-102.11	-212.80
	1.14	-126.36	-244.56	-110.96	-229.72	-123.75	-233.24	-110.86	-225.00

Table III: Values of in-medium mass-shift of  $\eta$ -meson for different medium attributes calculated in the ChPT+chiral model are tabulated (in units of MeV).

the in-medium mass-shift of  $\eta$ -meson at zero momentum in table II.

### B. In-medium Mass of $\eta$ Meson in Unified Approach of ChPT and Chiral Model

In this section, we have used the unified approach of chiral SU(3) model and chiral perturbation theory to calculate the medium induced mass of  $\eta$ -meson. As discussed in the methodology section, the  $\eta N$  equation of motion is obtained from the Lagrangian density of ChPT. Further, the scalar density of nucleons appearing in the ChPT equation of motion is obtained from the chiral SU(3) model. In this calculation, we have taken the value of parameter  $\Sigma_{\eta N}$  to be 280 MeV. We have not considered the contribution of uncertainties in the  $\Sigma_{\eta N}$  parameter because of the less contribution of sigma term in the in-medium mass as compared to  $\kappa$  term which we will see later. The value of in-medium  $\eta$  mass-shift calculated using present unified approach are given in table III.

In fig. 8, we illustrated the ratio of the in-medium and vacuum mass of the  $\eta$ -meson as a function of nuclear density. In this figure, we have also included the effect of  $\eta N$  scattering length, temperature, and medium isospin asymmetry. Moreover, we compared the results obtained from two different approaches *i.e.* (i) chiral model alone (ii) ChPT and chiral model. Using the second approach, we observed a substantial decrease in the mass of  $\eta$ -meson. We observed the same behavior of the in-medium mass with respect to temperature, asymmetry, and scattering length as was observed in the situation when the chiral model was used alone. The main difference is, in the ChPT the  $\eta$  meson gets a more net attractive contribution than the chiral model which is due to the absence of first range term in ChPT Lagrangian. In fig. 9 we have plotted the contributions of individual terms to the in-medium mass of  $\eta$ -

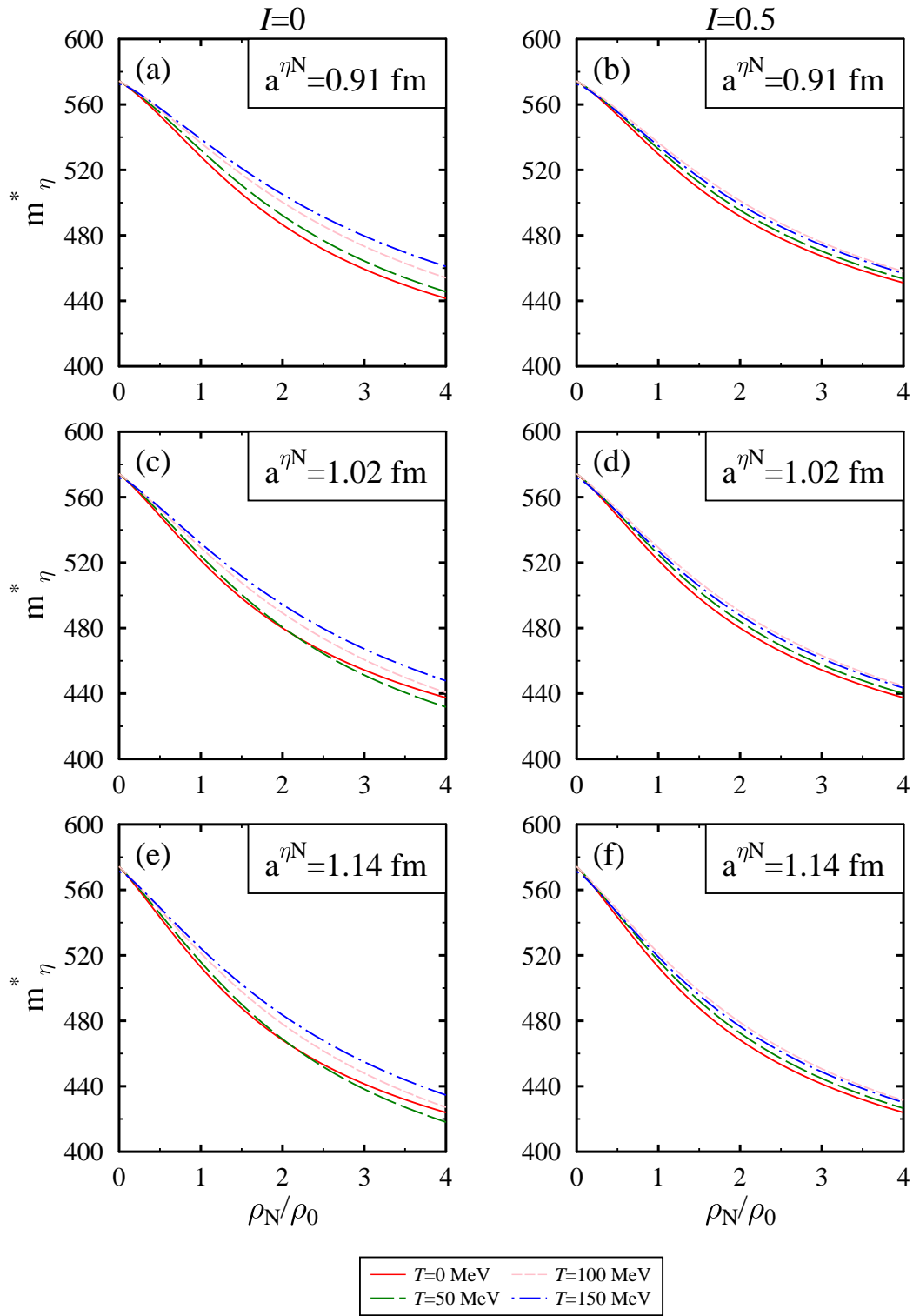


Figure 2: (Color online) In-medium  $\eta$  meson mass in the chiral model.

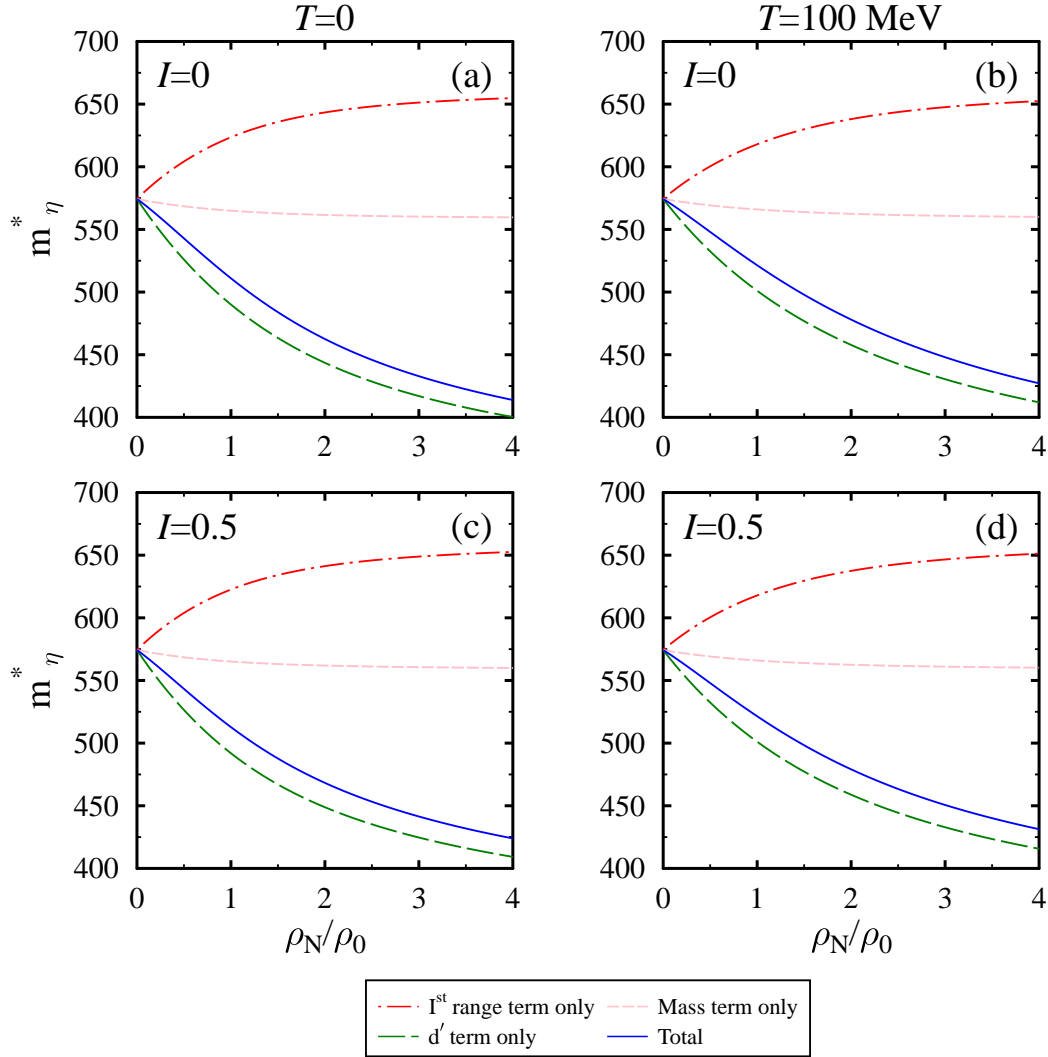


Figure 3: (Color online) Comparison of the different terms of  $\eta$ -meson effective mass in chiral model at  $a^{\eta N} = 1.14$  fm.

meson calculated from the unified approach. The  $\eta$ -meson in-medium mass given by Eq.(37) in the ChPT+chiral model approach has two terms (i)  $\Sigma_{\eta N}$  term and (ii)  $\kappa$  term. In this figure, we have shown the individual contribution of these terms with increasing nuclear density and observed a non-appreciable contribution with  $\Sigma_{\eta N}$  but appreciable with  $\kappa$  term. This is because in the  $\eta$ -meson in-medium mass expression (see Eq.(37)), the denominator has a positive contribution of the scalar densities and the increase in scalar density with

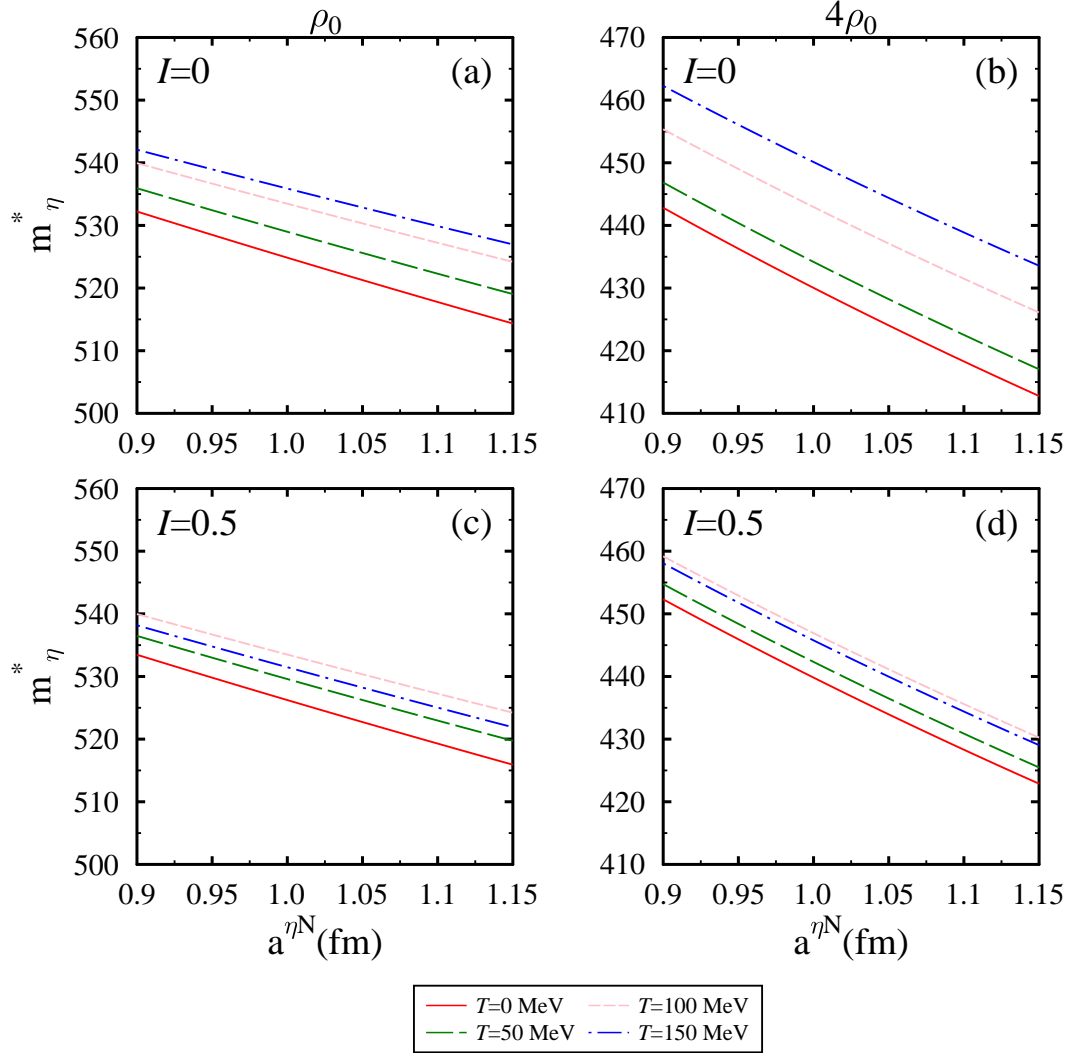


Figure 4: (Color online) The in-medium  $\eta$ -meson mass as a function of scattering length.

number density increases the denominator hence the value of effective mass becomes more negative. Clearly, there is no first range term with the positive contribution as was observed in the previous chiral model calculations, and therefore in the present case we get substantial attractive mass-shift.

The present observations can be compared with the  $\eta$ -meson effective mass calculated in the unified approach of ChPT and relativistic mean-field model of Ref. [10]. In this article, authors also considered the effect of scattering length and at nuclear saturation density and

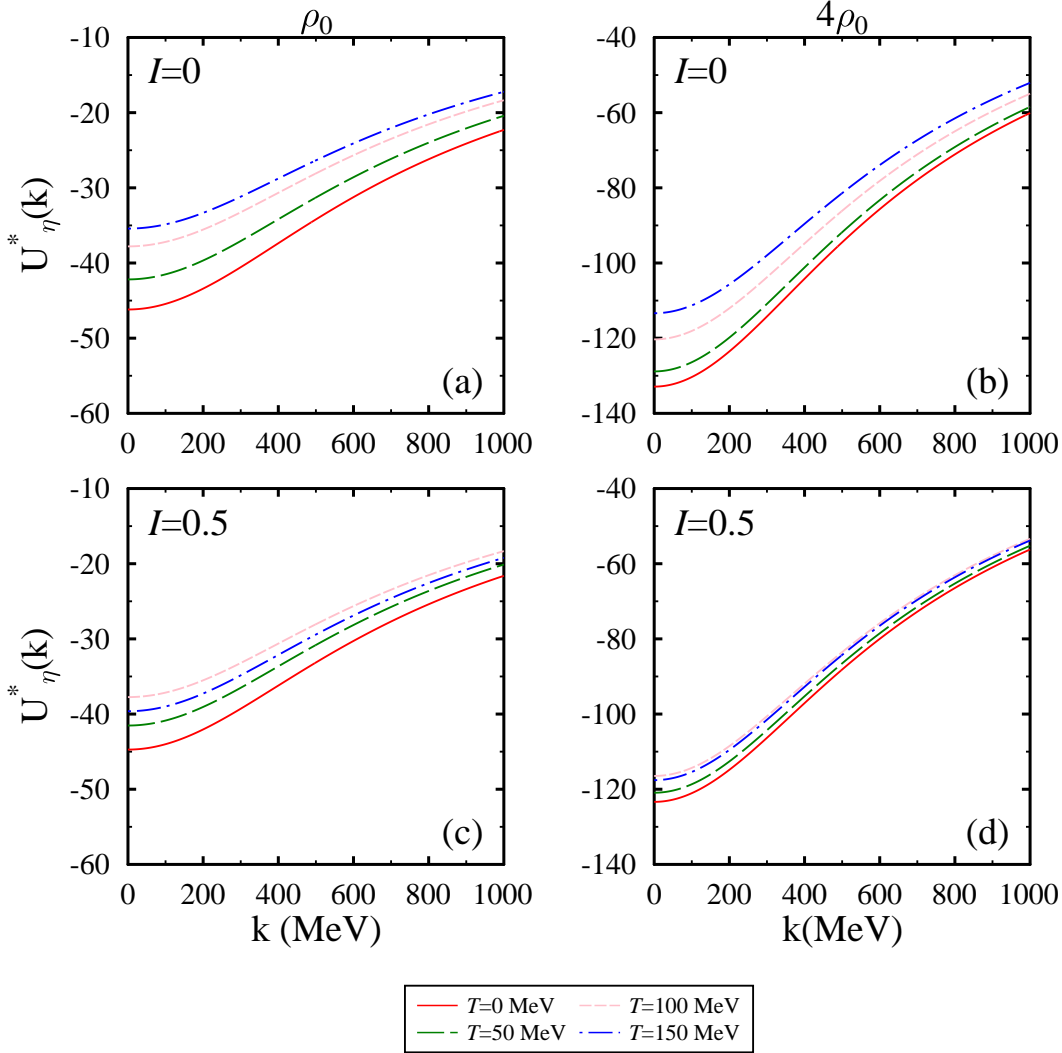


Figure 5: (Color online) The in-medium  $\eta$  meson optical potential in chiral model at  $a^{\eta N}=0.91$  fm.

$a^{\eta N}=1.02$  fm they anticipated the effective mass to be  $0.84 m_\eta$  whereas we observed it to be  $0.79 m_\eta$ . At nuclear saturation density, the effective mass equal to  $0.95 m_\eta$  was obtained within the coupled channel approach with scattering length  $a^{\eta N} \sim 0.25$  fm [11]. In this non-diagonal coupled channel approach, there are only leading order contributions and hence, only a small decrement in the in-medium mass is observed. Also, in the QMC model at  $\rho_0$  the in-medium mass of  $\eta$ -meson having value  $0.88 m_\eta$  was observed [45]. The obtained values are comparable with the calculations of the ChPT+chiral model for  $a^{\eta N} \sim 0.50$  fm.

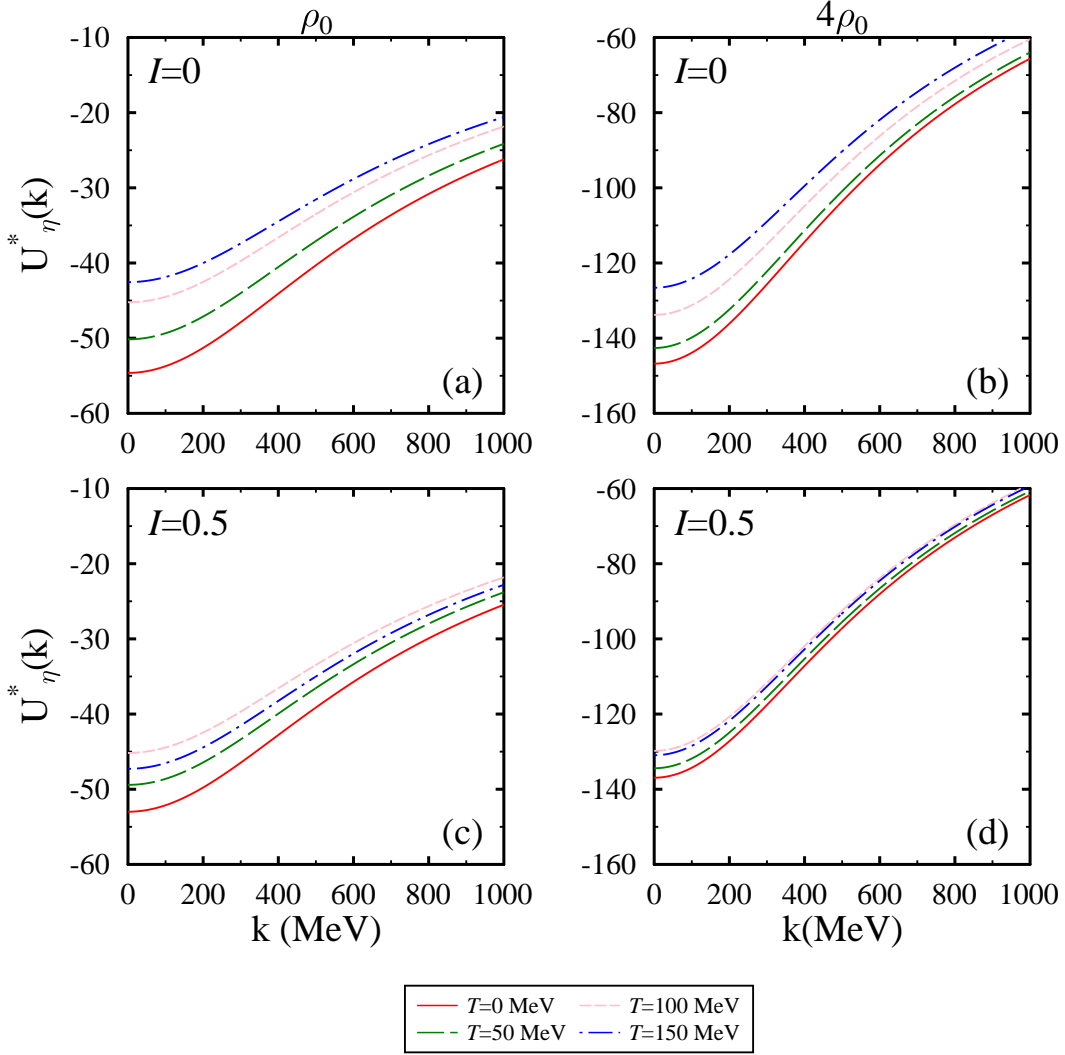


Figure 6: (Color online) The in-medium  $\eta$  meson optical potential in chiral model at  $a^{\eta N}=1.02$  fm.

In the cold symmetric nuclear matter, at  $\rho_N=\rho_0(4\rho_0)$  and  $|\mathbf{k}|=0$ , we observe optical potential to be -116.83 (-232.28) MeV for  $a^{\eta N}=1.02$  fm and in the cold isospin asymmetric nuclear matter the values modifies to -114.35 (-220.99) MeV. Using the ChPT+chiral model approach, we observed a even deeper optical potential than evaluated in the relativistic mean-field model+ChPT approach of Ref. [10]. This is due to the difference in the in-medium scalar densities obtained in two models. In our approach, we have taken the effect of scalar and vector fields under the influence of isospin asymmetry, and finite temperature

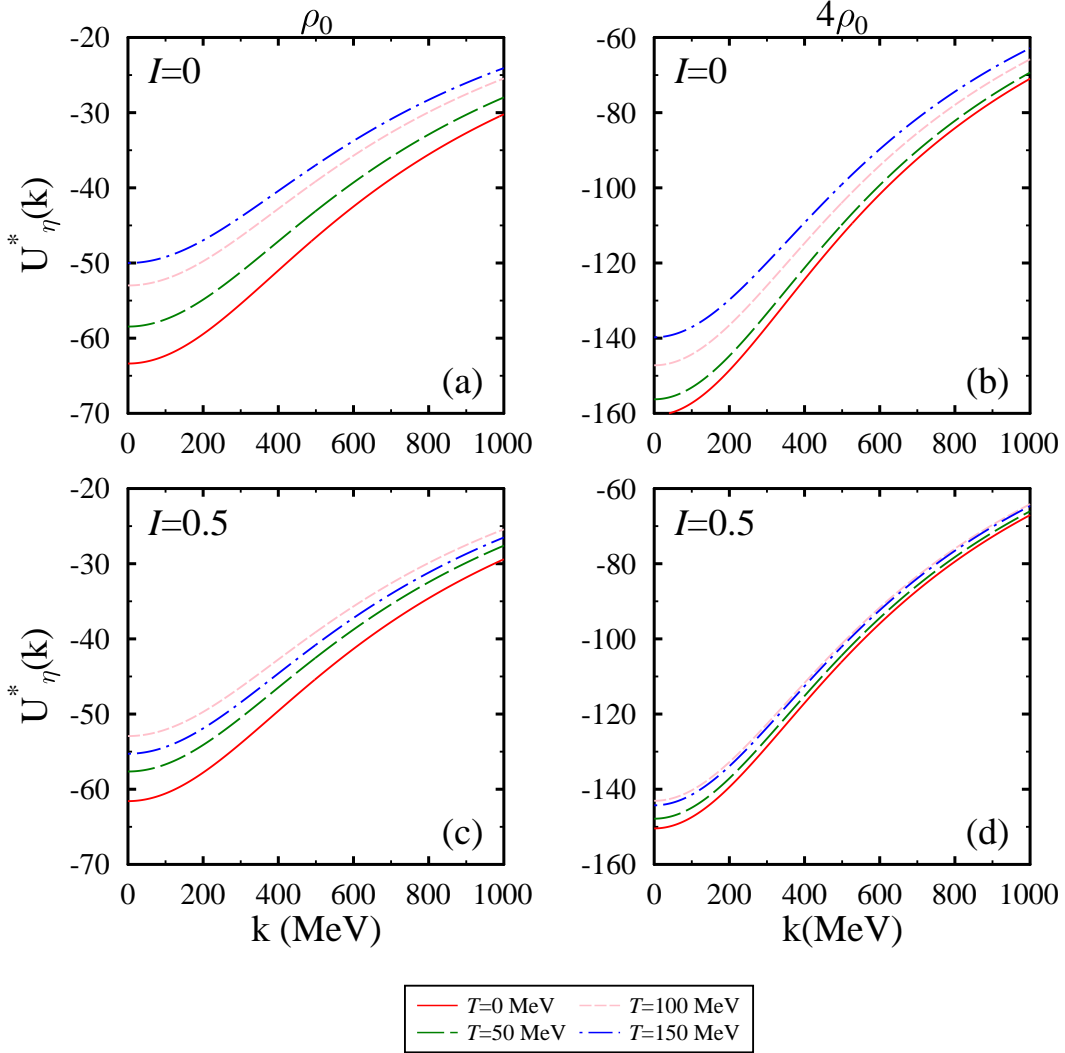


Figure 7: (Color online) The in-medium  $\eta$  meson optical potential in chiral model at  $a^{\eta N}=1.14$  fm.

whereas in the relativistic model approach only cold symmetric medium was considered. The  $\eta$  optical potential was also observed in the different theoretical observations [9–11, 45, 46].  $U_{\eta}=-34$  MeV was observed by studying the  $\eta N$  interactions near the threshold using free space chirally inspired coupled channel approach by considering the contributions of  $N^*(1535)$  baryon resonance [9]. Besides, the optical potential  $U_{\eta}=-54$ ,  $-60$ , and  $-83$  MeV was observed in the chiral unitary approach [46], QMC model [45], and the ChPT [10], respectively.

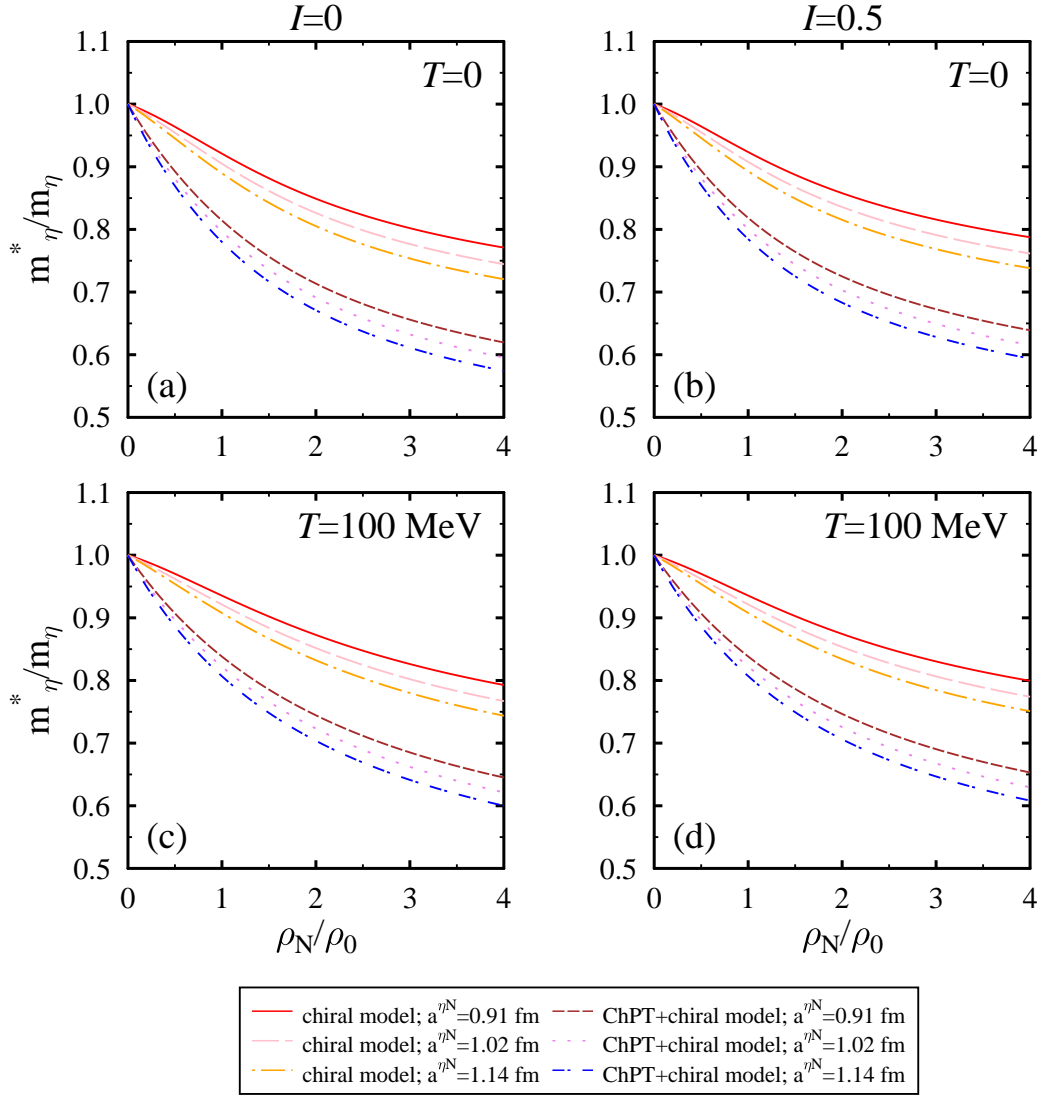


Figure 8: (Color online) Comparison of in-medium  $\eta$  meson mass calculated from chiral model and ChPT.

#### IV. SUMMARY

We investigated the in-medium mass of  $\eta$ -meson in the asymmetric nuclear matter at finite temperature. Under these medium conditions, we studied the behavior of the  $\eta$ -meson using two different methodologies. In the first methodology, using the chiral model alone we calculated the medium modified mass and optical potential of  $\eta$ -meson by considering the  $\eta N$  interactions up to second order in the Lagrangian and observe a decrease in the



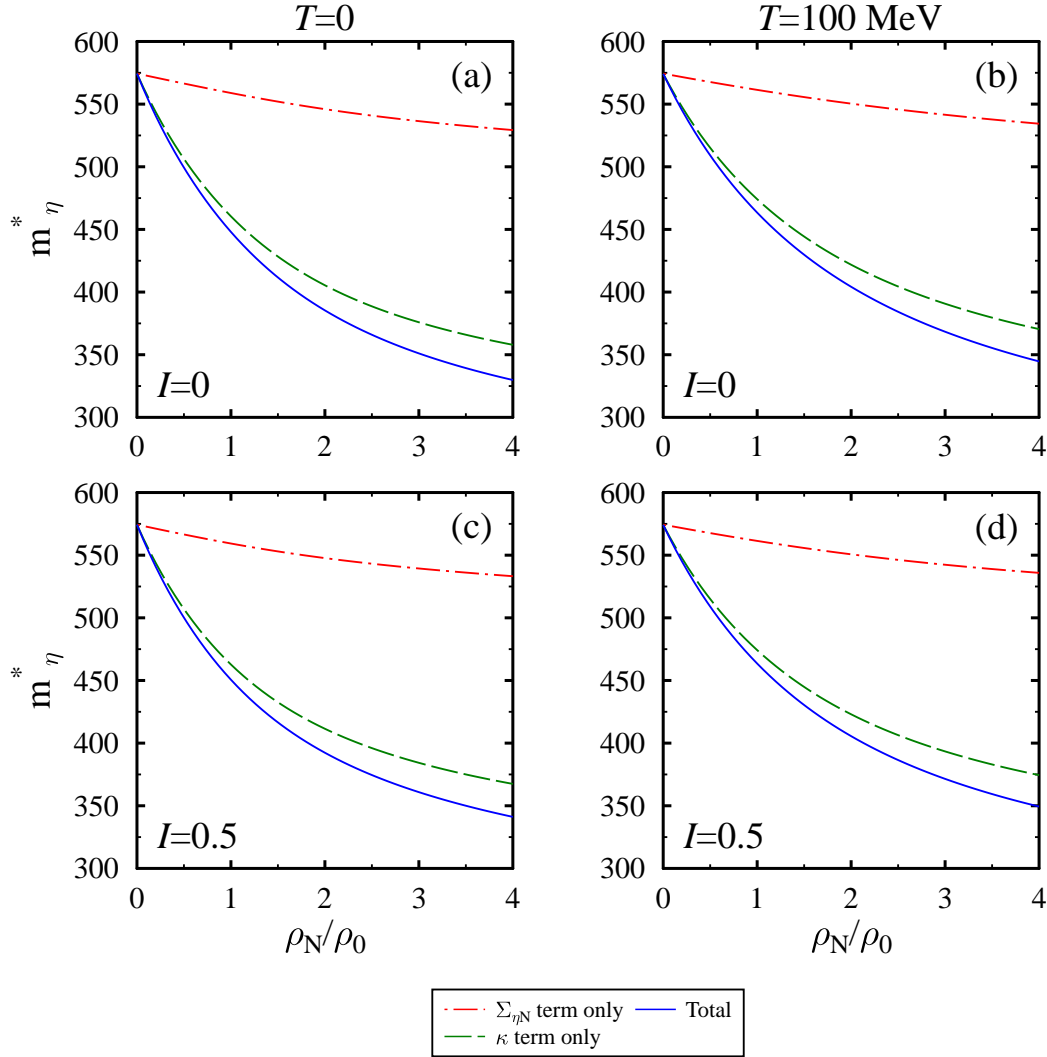


Figure 9: (Color online) Comparison of different terms of the effective mass of  $\eta$ -meson calculated using unification of ChPT and chiral model at  $a^{\eta N} = 1.14$  fm.

effective mass of  $\eta$ -meson as a function of density. We find the in-medium effects to be more appreciable in the high density regime. In the second, we used the unified approach of chiral perturbation theory (ChPT) and chiral SU(3) model to study the in-medium attributes of  $\eta$ -meson. In this approach, we took the next-to-leading order contributions. We incorporated the medium effects from the chiral SU(3) model through scalar density which is plugged in the  $\eta N$  equation of motion, which is calculated from the effective  $\eta N$  Lagrangian of ChPT.

Using this methodology, we find a substantial decrease in the mass of  $\eta$ -meson as a function of nuclear density. The temperature and asymmetry effects are also studied and found to be slight repulsive in nature. Also, in the both approaches the mass-shift is observed to increase with an increase in the value of scattering length. The decrement on the  $\eta$ -meson mass leads to a negative mass-shift/optical potential which further suggests the possibility of  $\eta N$  bound states. The optical potential calculated in the present work will be used in future to calculate the spectroscopic state of the  $\eta$ -mesic nuclei [10]. Also, the momentum dependent optical potential can be used to study the  $\eta$ -meson production rate [49–51] and its momentum dependence in the asymmetric nuclear medium [52, 84, 85].

### Acknowledgment

One of the authors, (R.K) sincerely acknowledge the support towards this work from Ministry of Science and Human Resources Development (MHRD), Government of India via Institute fellowship under National Institute of Technology Jalandhar.

### Appendix A: EXPLICIT REPRESENTATION OF DIFFERENT MATRICES

Here, we give the matrix representation of meson, baryon and mass matrices which are used in present calculations [2].

- The Scalar Meson Matrix,  $X$ :

$$X = \frac{1}{\sqrt{2}}\sigma^a\lambda_a = \begin{pmatrix} (\delta + \sigma)/\sqrt{2} & \delta^+ & \kappa^+ \\ \delta^- & (-\delta + \sigma)/\sqrt{2} & \kappa^0 \\ \kappa^- & \bar{\kappa}^0 & \zeta \end{pmatrix}. \quad (\text{A1})$$

- The Pseudoscalar Meson Matrix,  $P$ :

$$P = \frac{1}{\sqrt{2}}\pi_a\lambda^a = \begin{pmatrix} \frac{1}{\sqrt{2}}\left(\pi^0 + \frac{\eta}{\sqrt{1+2w^2}}\right) & \pi^+ & 2\frac{K^+}{w+1} \\ \pi^- & \frac{1}{\sqrt{2}}\left(-\pi^0 + \frac{\eta}{\sqrt{1+2w^2}}\right) & 2\frac{K^0}{w+1} \\ 2\frac{K^-}{w+1} & 2\frac{\bar{K}^0}{w+1} & -\frac{\eta\sqrt{2}}{\sqrt{1+2w^2}} \end{pmatrix}, \quad (\text{A2})$$

where  $w = \sqrt{2}\zeta_0/\sigma_0$ .

- The  $A_p$  Matrix:

$$A_p = \frac{1}{\sqrt{2}} \begin{pmatrix} m_\pi^2 f_\pi & 0 & 0 \\ 0 & m_\pi^2 f_\pi & 0 \\ 0 & 0 & 2m_K^2 f_K - m_\pi^2 f_\pi \end{pmatrix}. \quad (\text{A3})$$

- The Baryon Matrix,  $B$ :

$$B = \frac{1}{\sqrt{2}} b^a \lambda_a = \begin{pmatrix} \frac{\Sigma^0}{\sqrt{2}} + \frac{\Lambda^0}{\sqrt{6}} & \Sigma^+ & p \\ \Sigma^- & -\frac{\Sigma^0}{\sqrt{2}} + \frac{\Lambda^0}{\sqrt{6}} & n \\ \Xi^- & \Xi^0 & -2\frac{\Lambda^0}{\sqrt{6}} \end{pmatrix}. \quad (\text{A4})$$

- [1] L. Tolos and L. Fabbietti, Progress in Particle and Nuclear Physics **112**, 103770, (2020).
- [2] P. Papazoglou *et.al.*, Phys. Rev. C **59**, 411 (1999).
- [3] Arata Hayashigaki, Phys. Lett. B **487**, 96 (2000).
- [4] D. B. Kaplan and A. E. Nelson, Phys. Lett. B **175**, 57 (1986).
- [5] E. Jenkins and A. Manohar, Phys. Lett. B **255**, 558 (1991); **259**, 353 (1991).
- [6] L. Tolós *et.al.*, Phys. Rev. C **763**, 025203 (2004).
- [7] L. Tolós *et.al.*, Phys. Lett. B **635**, 85 (2006).
- [8] L. Tolós *et.al.*, Phys. Rev. C **77**, 015207 (2008).
- [9] A. Cieply *et.al.*, Nucl. Phys. A **925**, 126 (2014).
- [10] X. H. Zhong *et.al.*, Phys. Rev. C **73**, 015205 (2006).
- [11] T. Waas and W. Weise, Nucl. Phys. A **625**, 287 (1997).
- [12] R. Vogt, *Ultra-relativistic Heavy-Ion collisions*, Elsevier (2007).
- [13] R. Rapp *et.al.*, Progress in Particle and Nuclear Physics, **65**, 209 (2010).
- [14] Y. Nambu and G. Jona-Lasinio, Phys. Rev. **122**, 345 (1961).
- [15] K. Fukushima, Phys. Lett. B **591**, 277 (2004).
- [16] K. Kashiwa *et.al.*, Phys. Lett. B **662**, 26 (2008)
- [17] S. K. Ghosh *et.al.*, Phys. Rev. D **91**, 054005 (2015).
- [18] J. Hofmann and M.F.M. Lutz, Nucl. Phys. A **763**, 90 (2005).

- [19] A. Mishra *et.al.*, Phys. Rev. C **69**, 024903 (2004).
- [20] A. Mishra and S. Schramm, Phys. Rev. C **74**, 064904 (2006).
- [21] Arvind Kumar and Amruta Mishra, Phys. Rev. C **82**, 045207 (2010).
- [22] Arvind Kumar and Amruta Mishra, Eur. Phys. J. A **47**, 164 (2011).
- [23] Rajesh Kumar and Arvind Kumar, Phys. Rev. C **101**, 015202 (2020).
- [24] Rajesh Kumar and Arvind Kumar, Eur. Phys. J C **79**, 403 (2019).
- [25] Rajesh Kumar and Arvind Kumar, Chin. Phys. C **43**, 12 (2019).
- [26] Rajesh Kumar and Arvind Kumar, Phys. Rev. C **102**, 045206 (2020).
- [27] A. Mishra *et.al.*, Phys. Rev. C **69**,015202 (2004).
- [28] A. Mishra *et.al.*, Eur. Phys. J. A **41**, 205 (2009).
- [29] P.A.M. Guichon, Phys. Lett. B **200**, 235 (1988).
- [30] S. W. Hong and B. K. Jennings, Phys. Rev. C **64**, 038203 (2001).
- [31] K. Tsushima *et.al.*, Phys. Rev. C **59**, 2824 (1999).
- [32] A. Sibirtsev *et.al.*, Eur. Phys. J. A **6**, 351 (1999).
- [33] K. Saito and A.W. Thomas, Phys. Lett. B **327**, 9 (1994).
- [34] P. K. Panda *et.al.*, Phys. Rev. C **56**, 3134 (1997).
- [35] S. Chatterjee and K. A. Mohan, Phys. Rev. D **85**, 074018 (2012).
- [36] B. J. Schaefer *et.al.*, Phys. Rev. D **81**, 074013 (2010).
- [37] L.J. Reinders *et.al.*, Nucl. Phys. B **186**, 109 2(1981).
- [38] T. Hilger *et.al.*, Phys. Rev. C **79**, 025202 (2009).
- [39] L.J. Reinders *et.al.*, Phys. Reports **127**, 1 (1985).
- [40] F. Klingl *et.al.*, Nucl. Phys. A **624**, 527 (1997).
- [41] Frank Klingl *et.al.*, Phys. Rev. Lett. **82**, 3396 (1999).
- [42] Q. Haider and L. C. Liu, Phys. Lett. B **172**, 257 (1986).
- [43] Liu and Q. Haider, Phys. Rev. C **34**, 1845 (1986).
- [44] H. C. Chiang *et.al.*, Phys. Rev. C **44**, 738 (1991).
- [45] K. Tsushima *et.al.*, Phys. Lett. B **443**, 26 (1998).
- [46] T. Inoue and E. Oset, Nucl. Phys. A **710**, 354 (2002).
- [47] Wang Teng-Teng, Chin. Phys. C **34**, 460 (2010).
- [48] C. Y. Song *et.al.*, EuroPhysics Letters **81**, 4 (2008).
- [49] J.C. Peng *et.al.*, Phys. Rev. Lett. **58**, 2027 (1987).

- [50] G. Martinez *et.al.*, Phys. Rev. Lett. **83**, 1538 (1999).
- [51] G. Agakishiev *et.al.*, Phys. Rev. C **88**, 024904 (2013).
- [52] F.-D. Berg *et.al.*, Phys. Rev. Lett. **72**, 977 (1994).
- [53] E. Chiavassa *et.al.*, Europhys. Lett. **41**, 365 (1998).
- [54] R. Averbeck *et.al.*, Phys. Rev. C **67**, 024903 (2003).
- [55] D. Zschesche *et.al.*, Phys. Rev. C **70**, 045202 (2004).
- [56] Rajesh Kumar *et.al.*, Eur. Phys. J A **56**, 278 (2020).
- [57] Arvind Kumar, Adv. High Energy Phys. **2014**, 549726 (2014).
- [58] Rahul Chhabra and Arvind Kumar, Eur. Phys. J. A **53**, 105 (2017).
- [59] Rahul Chhabra and Arvind Kumar, Eur. Phys. J. C **77**, 726 (2017).
- [60] Rahul Chhabra and Arvind Kumar, Phys. Rev. C **98**, 025205 (2018).
- [61] G. E. Brown *etal.*, Nucl. Phys. A **567**, 937 (1994).
- [62] C. H. Lee *etal.*, Nucl. Phys. A **585**, 401 (1995).
- [63] N. Kaiser *etal.*, Nucl. Phys. A **594**, 325 (1995).
- [64] Steven Weinberg, Phys. Rev. **166**, 1568, 1968.
- [65] S. Coleman *et.al.*, Phys. Rev. **177**, 2239 (1969).
- [66] D. Zschesche, *Description of Hot, Dense, and Strange Hadronic Matter in a Chiral  $SU(3)_L \times SU(3)_R$   $\sigma$ -Model*, Diploma Thesis, Goethe University Frankfurt (1997).
- [67] W. A. Bardeen and B. W. Lee, Phys. Rev. **177**, 2389 (1969).
- [68] I. Zakout *et.al.*, Phys. Rev. C **61**, 055208 (2000).
- [69] P. Wang *et.al.*, Nucl. Phys. A **688**, 791, (2001).
- [70] Sushruth Reddy P. *et.al.*, Phys. Rev. C **97**, 065208 (2018).
- [71] P.A. Zyla *et al.* [Particle Data Group], PTEP **2020**, no.8, 083C01 (2020).
- [72] L. Burakovsky, T. Goldman, [arXiv:hep-ph/9708498v1](https://arxiv.org/abs/hep-ph/9708498) (1997).
- [73] A. Mishra *et.al.*, Phys. Rev. C **78**, 024901 (2008).
- [74] T-S. Park *et.al.*, Phys. Rep. **233**, 341 (1993).
- [75] V. E. Lyubovitskij *et.al.*, Phys. Rev. D **63**, 054026 (2001).
- [76] S. J. Dong *et.al.*, Phys. Rev. D **54**, 5496 (1996).
- [77] T. Hatsuda and T. Kunihiro, Phys. Rep. **247**, 221 (1994).
- [78] H. Georgi, Weak interactions and modern particle theory (Benjamin/Cummings, Menlo Park, CA, 1984).

- [79] H.D. Politzer and M.B Wise, Phys. Lett. B **273**, 156 (1991).
- [80] A.M. Green and S. Wycech, Phys. Rev. C **71**, 014001 (2005).
- [81] F. Renard *et al.*, Phys. Lett. B **528**, 215 (2002).
- [82] R. A. Arndt *et.al.*, Phys. Rev. C **72**, 045202 (2005).
- [83] A. M. Green and S. Wycech, Phys. Rev. C **60**, 035208 (1999).
- [84] Jie Chen *et.al.*, Eur. Phys. J A **53**, 128 (2017).
- [85] J. C. David *et.al.*, Eur. Phys. J Plus **133**, 253 (2018).